Chiral corrections to the axial charges of the octet baryons from quenched QCD

Myunggyu Kim

Electronics and Telecommunications Research Institute (ETRI), Taejon 305-350, Korea

Seyong Kim

Department of Physics, Sejong University, Seoul 143-747, Korea

Using quenched chiral perturbation theory, we calculate one-loop corrections to the axial charges of the octet baryons in the quenched approximation to quantum chromodynamics. The results are used to compare chiral corrections to the axial charges in full QCD chiral perturbation theory with those in quenched QCD. We find that the quenched chiral perturbation theory result $c_0^Q + (c_{l0}^Q + c_{l2}^Q m_\pi^2) \ln m_\pi^2 + c_2^Q m_\pi^2 + \cdots$ is singular in the chiral limit unlike the regular behavior of the full QCD chiral perturbation theory result $c_0 + c_{l2} m_\pi^2 \ln m_\pi^2 + \cdots$. [S0556-2821(98)07517-1]

I. INTRODUCTION

Lattice quantum chromodynamics (QCD) simulation allows us to investigate the low-energy phenomena of strong interactions using first principles of quantum field theory. It is well suited for understanding the nonperturbative nature of strong interactions. Thus far, this method has been successfully employed in calculating various low-energy QCD related quantities [1].

However, many physical observables are calculated in lattice QCD using the so-called ''quenched approximation'' in which vacuum polarization effects coming from quark-antiquark pair creation and annihilation are neglected. This approximation is used because of the extensive computational cost in full QCD lattice simulations in particular of the light quark system. Such truncation, otherwise in a first principle calculation, can cause undesirable effects. First of all, it is difficult to estimate quantitatively systematic errors induced by the truncation. Second, since most cases of current lattice simulations are done with bare quark masses which produce pion masses heavier than the experimental value, heavier mass results from simulations must be extrapolated to the experimental pion mass region. Usually, a linear or quadratic fit has been used for the chiral extrapolation. Such an extrapolation may not be appropriate in quenched QCD (QQCD) because nonanalytic terms in the chiral expansion due to pion loops in quenched QCD will be different from those in full QCD.

In order to understand quenching effects on the chiral limit of various physical observables in light quark systems, Sharpe devised a rule + diagrammatic method [2]. Bernard and Golterman [3] developed a systematic way based on the symmetry of QQCD extending earlier work [4]. The latter method is in a similar spirit to chiral perturbation theory and an application of the same idea to the baryonic system was constructed by Labrenz and Sharpe [5]. By use of these methods, it is found that the chiral behaviors of many physical quantities in QQCD are different than those in full QCD and there are indeed differences caused by the quenched approximation. One may ask whether such differences are numerically noticeable in the physical pion mass region. If the deviation is small in the physical mass region, we may safely neglect it. For the pion mass, numerical investigations revealed that although there is a difference between the chiral behavior of full QCD and that of QQCD, it is either small at the physical pion mass region [6,7] or may be caused by the finite lattice volume [8]. The quenching effect on each baryon mass is numerically small although quenching effect on the baryon mass splitting is significant [9].

Of course, there are many more quantities where the quenched approximation introduces noticeable differences (e.g., the heavy-light meson system [10,11], pion scattering length [12], etc.) which await numerical investigation. Here, using the method developed in Ref. [5], we suggest that the chiral behavior of the axial charge of the octet baryons in QQCD should depart noticeably from that of full QCD in the physical pion mass region, provided that the same couplings and the same cutoff are chosen for both QQCD and full QCD. In this case, a quenched calculation may not be trusted, let alone a linear extrapolation of quenched lattice QCD simulation results.

In Sec. II, we briefly explain the quenched chiral perturbation theory described in Ref. [5] where the baryon fields are introduced via the heavy baryon formulation. Section III explains our calculations of the axial current matrix elements for the octet baryons. In Sec. IV we discuss some implications of our results. In Appendix A expressions for the coefficients defined in the axial current renormalizations are listed.

II. QUENCHED CHIRAL PERTURBATION THEORY WITH BARYONS

In the following, we briefly mention the essential ingredients of quenched chiral perturbation theory (QχPT). Details are available in Refs. [3,5] and we follow the notations in Ref. [5]. The quenched approximation amounts to neglecting the quark determinant. Canceling the quark determinant can be achieved by introducing additional bosonic degrees of freedom $\tilde{q}_i$ corresponding to each flavor of the quark field q_i. Each $\tilde{q}_i$ has the same mass, charge, etc., as the original quark. Since the new bosonic degrees of freedom have the

same quantum number as fermion degrees of freedom (quarks) except the statistics, the Gaussian integral over the new degrees of freedom matches exactly the determinant from the quark degrees of freedom with the inverse of the determinant. Because of new bosonic degrees of freedom, the symmetry of QQCD becomes the graded symmetry $U(3|3) \times U(3|3)$ for the quenched system of light quarks $Q = (u, d, s, \tilde{u}, \tilde{d}, \tilde{s})$. This symmetry determines the form of the interactions among the pseudoscalar mesons in QχPT.

The dynamics of the meson sector is conveniently described by a Hermitian 6×6 matrix field Φ,

$$\Phi = \begin{bmatrix} \phi & \chi^\dagger \\ \chi & \tilde{\phi} \end{bmatrix}, \tag{2.1}$$

where ϕ is the ordinary meson, $\tilde{\phi}$ is the meson composed of bosonic quarks, and $\chi, \chi^\dagger$ is the fermionic meson. As in the chiral perturbation theory (χPT) for full QCD, the following is useful in constructing the effective Lagrangian for QQCD:

$$\Sigma(x) = e^{2i\Phi(x)/f}, \quad \xi(x) = e^{i\Phi(x)/f}, \tag{2.2}$$

$$A_\mu(x) = \frac{i}{2}(\xi \partial_\mu \xi^\dagger - \xi^\dagger \partial_\mu \xi), \quad V_\mu(x) = \frac{1}{2}(\xi \partial_\mu \xi^\dagger + \xi^\dagger \partial_\mu \xi). \tag{2.3}$$

Under $U(3|3) \times U(3|3)$, the meson fields transform as

$$\Sigma \to L\Sigma R^\dagger, \xi \to L\xi U^\dagger(x) = U(x)\xi R^\dagger. \tag{2.4}$$

A component Σ_{ij} has the same transformation properties as the operator $Q_i \bar{Q}_j$. The axial anomaly breaks this full chiral symmetry in the classical level, down to the semidirect product $[SU(3|3) \times SU(3|3)] \otimes U(1)$ in the quantum level. This reduction in the symmetry introduces the field $\Phi_0 = \text{str}(\Phi)/\sqrt{3} = (\eta' - \tilde{\eta}')/\sqrt{2}$ and allows the quenched chiral Lagrangian to include arbitrary functions of Φ_0. The resulting Lagrangian in the mesonic sector is then

$$\mathcal{L}_\phi^Q = \frac{f^2}{4}[\text{str}(\partial_\mu \Sigma \partial^\mu \Sigma^\dagger) V_1(\Phi_0)$$
$$+ 2\mu \, \text{str}(\xi^\dagger m \xi^\dagger + \xi m \xi) V_2(\Phi_0)]$$
$$+ \alpha_\Phi V_5(\Phi_0) \partial_\mu \Phi_0 \partial^\mu \Phi_0 - m_0^2 V_0(\Phi_0) \Phi_0^2, \tag{2.5}$$

where str denotes super trace [3,5] and $m = \text{diag}(m_u, m_d, m_s, m_u, m_d, m_s)$. The potentials are normalized as $V_i(\Phi_0) = 1 + \mathcal{O}(\Phi_0^2)$. In our calculations, the higher order terms in the potentials will not be needed since we are interested in leading order behaviors. In full chiral perturbation theory, the vertex $i(\alpha_\Phi p^2 - m_0^2)/3$ iterates infinitely in the η' propagator. Thus η' acquires heavy mass and can be integrated out of the effective Lagrangian. In the quenched theory, however, only one insertion of this vertex survives and the Φ_0 remains light. We must therefore keep the last two terms in $\mathcal{L}_\phi^q$ and this will introduce two additional parameters in the baryon sector unlike full theory and will induce more singular behaviors in the chiral limit of QQCD.

These new couplings α_Φ and m_0^2 break the usual power counting rule in χPT since higher loop diagrams involving these vertices are not suppressed by powers of p/Λ_χ or m_π/Λ_χ where Λ_χ is the chiral cutoff. However, since the actual expansion parameters in loop calculations are $\alpha_\Phi/3$ and $m_0^2/3$, we assume that $\alpha_\Phi/3$ and $(m_0/\Lambda_\chi)^2/3$ are small and calculate only the leading behavior in these coupling [3,5].

The following is a brief summary of the method described in Ref. [5], on how to extend the above idea for the meson fields to the baryon fields in QQCD. QQCD has $qq\tilde{q}$, $q\tilde{q}\tilde{q}$, and $\tilde{q}\tilde{q}\tilde{q}$ baryons, in addition to the usual qqq baryons. To construct irreducible representations of $SU(3|3)_V$ for QQCD, we guide ourselves by the baryon field representations in QCD and begin with the "quark" field Q and its conjugate "antiquark" field $\bar{Q}$, defined the above. These $Q, \bar{Q}$ fields transform as a fundamental representation and its conjugate representation of $SU(3|3)_V$. Using three Q's, we define spin-1/2 baryons

$$B_{ijk}^\gamma \sim [Q_i^{\alpha,a} Q_j^{\beta,b} Q_k^{\gamma,c} - Q_i^{\alpha,a} Q_j^{\gamma,c} Q_k^{\beta,b}]\varepsilon_{abc}(C\gamma_5)_{\alpha\beta}, \tag{2.6}$$

in analogy to spin-1/2 baryon fields in full theory

$$\mathcal{B}_{ijk}^{\text{full}} \sim [q_i^{\alpha,a} q_j^{\beta,b} q_k^{\gamma,c} - q_i^{\alpha,a} q_j^{\gamma,c} q_k^{\beta,b}]\varepsilon_{abc}(C\gamma_5)_{\alpha\beta}, \tag{2.7}$$

and for spin-3/2 baryons, we define

$$T_{\alpha,ijk}^\mu \sim [Q_i^{\alpha,a} Q_j^{\beta,b} Q_k^{\gamma,c} + Q_i^{\beta,b} Q_j^{\gamma,c} Q_k^{\alpha,a}$$
$$+ Q_i^{\gamma,c} Q_j^{\alpha,a} Q_k^{\beta,b}]\varepsilon_{abc}(C\gamma_\mu)_{\beta\gamma} \tag{2.8}$$

in analogy to spin-3/2 baryon fields in full theory

$$\mathcal{T}_{ijk}^{\text{full}} \sim [q_i^{\alpha,a} q_j^{\beta,b} q_k^{\gamma,c} + q_i^{\beta,b} q_j^{\gamma,c} q_k^{\alpha,a}$$
$$+ q_i^{\gamma,c} q_j^{\alpha,a} q_k^{\beta,b}]\varepsilon_{abc}(C\gamma_\mu)_{\beta\gamma}, \tag{2.9}$$

where $C = i\gamma_2\gamma_0$ is the charge conjugation matrix and a, b, and c are color indices. Both fields have the same transformation properties

$$B_{\gamma,ijk}(T_{\alpha,ijk}^\mu) \to (-)^{i'(j+j')+(i'+j')(k+k')}$$
$$\times U_{ii'} U_{jj'} U_{kk'} B_{\gamma,i'j'k'}(T_{\alpha,i'j'k'}^\mu), \tag{2.10}$$

where $U \in SU(3|3)_V$, and these transformation properties make B and T representations of $SU(3|3)_V$. Due to the fact that the off-diagonal 3×3 blocks of U are Grassmann variables, there are sign factors (grading factors). The notations for the indices in the sign factors are as follows: one for the anticommuting variables ($i = 1, 2, 3$) and zero for the commuting variables ($i = 4, 5, 6$). The spin-3/2 baryon fields are completely symmetric under flavor index exchanges and this makes it easy to see that they are irreducible representations $SU(3|3)_V$. Constructing the spin-1/2 baryon fields are more involved. It is true even in the full QCD case since spin-1/2
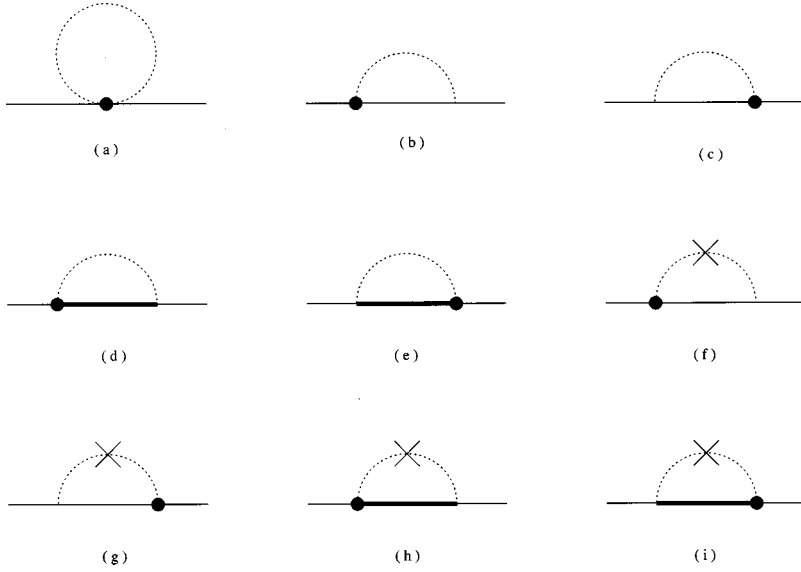
FIG. 1. Vanishing graphs. The solid dots represent the vertices stemming from the axial current.

baryon fields are mixed representations of SU(3) flavor symmetry of full QCD: in Eq. (2.8), among three flavor indices of qqq, the first two are antisymmetric under the exchange and the third one is symmetric under the exchange with any of the first two indices. Thus, the second term in the construction of spin-1/2 baryons in quenched theory is needed to make the representation irreducible under $SU(3|3)_V$ [5].

These QQCD baryon fields satisfy the symmetry properties

$$B_{ijk} = (-)^{jk+1} B_{ikj},$$

$$B_{ijk} + (-)^{ij+1} B_{jik} + (-)^{ij+jk+ki+1} B_{kji} = 0,$$

$$T_{ijk}^\mu = (-)^{ij+1} T_{jik} = (-)^{jk+1} T_{ikj} \tag{2.11}$$

because of the grading factors. The above two lines make spin-1/2 baryon fields irreducible representations of $SU(3|3)_V$ with dimension 70. The first condition gives $6 \times \frac{1}{2} \times 5 \times 6$ independent states and the $6!/(3!3!)$ constraints from the second condition reduces the total number of states to 70. The representation including spin-3/2 baryons is 38 dimensional. We call the baryons of the 70(38) simply ''octet''(''decuplet'') baryons since they contain an SU(3) octet (decuplet) when restricted to the index range 1–3.

The Lagrangian in the baryon sector in the lowest order can be written in terms of the invariants of bilinear baryon fields. They include the covariant derivative or the field A^μ in Eq. (2.3). The covariant derivative of the field B_{ijk} is given by

$$D^\mu B_{ijk} = \partial^\mu B_{ijk} + (V^\mu)_{ii'} B_{i'jk} + (-)^{i(j+j')} (V^\mu)_{jj'} B_{ij'k}$$

$$+ (-)^{(i+j)(k+k')} (V^\mu)_{kk'} B_{ijk'}, \tag{2.12}$$

where V^μ is a vector current defined by Eq. (2.3). The covariant derivative of the field T_{ijk}^μ takes the same form. We follow the notation of Ref. [5] for the contraction of the flavor indices. They are

$$\bar{C} \Lambda C' \equiv \bar{C}_{kji} \Lambda C'_{ijk}, \tag{2.13}$$

$$\bar{C} \Lambda E C' \equiv \bar{C}_{kji} \Lambda E_{ii'} C'_{i'jk}, \tag{2.14}$$

$$\bar{C} \Lambda C' E \equiv \bar{C}_{kji} \Lambda E_{kk'} C'_{ijk'} (-)^{(i+j)(k+k')}, \tag{2.15}$$

where C and C' are the baryon fields, E is a matrix field, and Λ is an arbitrary Dirac matrix. An example of E is A^μ.

The lowest order Lagrangian is, then,

$$\mathcal{L}^Q = \mathcal{L}_\Phi^Q + \mathcal{L}_{BT\Phi}^Q \tag{2.16}$$

where $\mathcal{L}_\Phi^Q$ is given in Eq. (2.5) and

$$\mathcal{L}_{BT\Phi}^Q = i\bar{B} v \cdot DB - i\bar{T}^\nu v \cdot DT_\nu + \Delta M \bar{T}^\nu T_\nu + 2\alpha \bar{B} S_\mu B A^\mu$$

$$+ 2\beta \bar{B} S_\mu A^\mu B + 2\gamma \bar{B} S_\mu B \, \mathrm{str}(A^\mu) + 2H \bar{T}^\nu S_\mu A^\mu T_\nu$$

$$- \sqrt{\frac{3}{2}} C [\bar{T}^\nu A^\nu B + \bar{B} A_\nu T^\nu] + 2\gamma' \bar{T}^\nu S_\mu T_\nu \, \mathrm{str}(A^\mu). \tag{2.17}$$

The symbols v and S^μ denote the fixed velocity and the spin operator in the heavy baryon formalism [13]. Various other possible terms such as $\bar{B}_{ijk} S^\mu A_{\mu,jj'} B_{ij'k} (-)^{i(j+j')}$, etc., are not independent due to the symmetry properties given in Eq. (2.11). In calculating contributions from the decuplet baryons, we assume that $\Delta M \ll m_\pi$ and treat the octet and the decuplet baryons as degenerate. Extending our calculation to the case $\Delta M \neq 0$ is easy. Its effect will be discussed in Sec. IV.

When the flavor indices are restricted to the range 1–3, the baryon fields in the quenched theory are explicitly related to ones in full theory as

$$B_{ijk}|_R = \frac{1}{\sqrt{6}} (\varepsilon_{ijk'} B_{k'k}^{\mathrm{full}} + \varepsilon_{ikk'} B_{k'j}^{\mathrm{full}}), \tag{2.18}$$

$$T_{ijk}|_R = T_{ijk}^{\text{full}}. \tag{2.19}$$

Using these relations, one can formally show that the quenched Lagrangian is equal to the full Lagrangian under the restrictions of the flavor indices and the identifications of the parameters

$$\alpha = 2\left(\frac{1}{3}D + F\right), \beta = \left(-\frac{5}{3}D + F\right), \gamma = 2(D-F), \tag{2.20}$$

although there is no reason why the parameters of two theories should be related to each other. For better comparison with χPT result, we will re-express our results using these relations except γ.

III. THE AXIAL CURRENT MATRIX ELEMENTS FOR THE OCTET BARYONS

The axial current from the quenched chiral Lagrangian is given by

$$
\begin{aligned}
J_\mu^a = &i\frac{f^2}{2}\text{str}[T^a(\partial_\mu\Sigma^\dagger\Sigma - \partial_\mu\Sigma\Sigma^\dagger)] + v_\mu[\bar{B}\Omega_-^A B + 2\bar{B}B\Omega_-^A \\
&+ 3\bar{T}^\nu\Omega_-^A T_\nu] + 2\alpha\bar{B}S_\mu B\Omega_+^A + 2\beta\bar{B}S_\mu\Omega_+^A B \\
&+ 2\gamma\bar{B}S_\mu B\text{str}(\Omega_+^A) + 2H\bar{T}^\nu S_\mu\Omega_+^A T_\nu \\
&+ 2\gamma'\bar{T}^\nu S_\mu T_\nu\text{str}(\Omega_+^A) - \sqrt{\frac{3}{2}}C(\bar{T}^\mu\Omega_+^A B + \bar{B}\Omega_+^A T^\mu),
\end{aligned}
\tag{3.1}
$$

$$\Omega_\pm^A = \frac{1}{2}(\xi T^A\xi^\dagger \pm \xi^\dagger T^A\xi), \tag{3.2}$$

$$T^A = \frac{1}{2}\begin{bmatrix}\lambda^A & 0 \\ 0 & \lambda^A\end{bmatrix}, \tag{3.3}$$

where λ^A are Gell-Mann matrices. The numerical factors 2 and 3 are due to the symmetry properties given in Eq. (2.11).

The renormalization of the axial current can be calculated by computing the diagrams given in Figs. 1, 2, and 3 using Feynman rules derived from $\mathcal{L}_\Phi^Q$, $\mathcal{L}_{BT\Phi}^Q$, and the vertices from Eq. (3.1). All the contributions from the diagrams in Fig. 1 vanish: (a) vanishes since only closed quark loops are present (which cannot exist in the quenched approximation) and the others are zero due to the property $v \cdot S = 0$. Then, the matrix element of J^A for the octet baryons B_i and B_j can be written in the form

$$
\begin{aligned}
\langle B_i|J^A|B_j\rangle = \bar{u}_{B_i}\gamma^\mu\gamma^5 u_{B_j}t_{ij}^A\Bigg[&1 + \sum_{a\leq b}(\alpha_{ij,ab}^A - \lambda_{ij,ab})X_{ab} \\
&+ \sum_{a\leq b}(\beta_{ij,ab}^A - \rho_{ij,ab})Y_{ab}\Bigg],
\end{aligned}
\tag{3.4}
$$
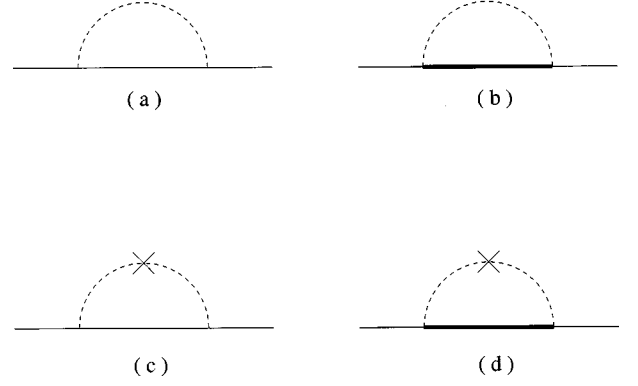
FIG. 2. Wave function renormalization graphs. The cross represents the vertex $i(\alpha_\Phi p^2 - m_0^2)/3$.

$$X_{ab} = \frac{M_{ab}^2}{16\pi^2 f^2}\ln\frac{M_{ab}^2}{\mu^2}, \tag{3.5}$$

$$Y_{ab} = \frac{(\alpha_\Phi M_{aa}^2 - m_0^2)X_{aa} - (\alpha_\Phi M_{bb}^2 - m_0^2)X_{bb}}{3(M_{aa}^2 - M_{bb}^2)}, \tag{3.6}$$

$$Y_{aa} = \frac{1}{48\pi^2 f^2}\Bigg[(2\alpha_\Phi M_{aa}^2 - m_0^2)\ln\frac{M_{aa}^2}{\mu^2} + (\alpha_\Phi M_{aa}^2 - m_0^2)\Bigg], \tag{3.7}$$

where t_{ij}^A is the tree level result, $\lambda_{ij,ab}$ and $\rho_{ij,ab}$ are the wave function renormalization factors without and with the hairpin vertex $[i\frac{2}{3}(\alpha_\Phi k^2 - m_0^2)]$, and $\alpha_{ij,ab}^A$ and $\beta_{ij,ab}^A$ are the one-loop corrections without and with the hairpin vertex. We list the coefficients in the Appendix. Here we work in the limit $m_u = m_d$. The μ is the scale introduced in the dimensional regularization. The scale dependence is canceled by the counterterms obtained by the $O(m_q)$ Lagrangian such as

$$\frac{(\mu^2)^{2-d/2}}{\Lambda_\chi}\bar{B}(\xi^\dagger m\xi^\dagger + \xi m\xi)S^\mu A_\mu B, \tag{3.8}$$

where m is the quark mass matrix. Including the counterterms, the function X_{ab} changes to

$$X_{ab} \to \frac{M_{ab}^2}{16\pi f^2}\Bigg[\ln\frac{M_{ab}^2}{\mu^2} + c(\mu)\Bigg], \tag{3.9}$$

where $c(\mu)$ is the counterterm. In the real world the logarithmic correction is not significantly large [14].

It is interesting to compare full chiral corrections with quenched chiral corrections for one of the above matrix elements (since we are interested in qualitative feature of the chiral limit, we take $\mu \simeq \Lambda_\chi \sim 1$ GeV and neglect the finite part in the following). We choose the isovector axial charge of the proton, g_A for the comparison since a quenched lattice simulation data for this quantity is available [15]. Also, for full χPT case, Jenkins and Manohar already computed one-loop chiral logarithmic contributions to the baryon axial vector currents with the intermediate states of the octet and de-
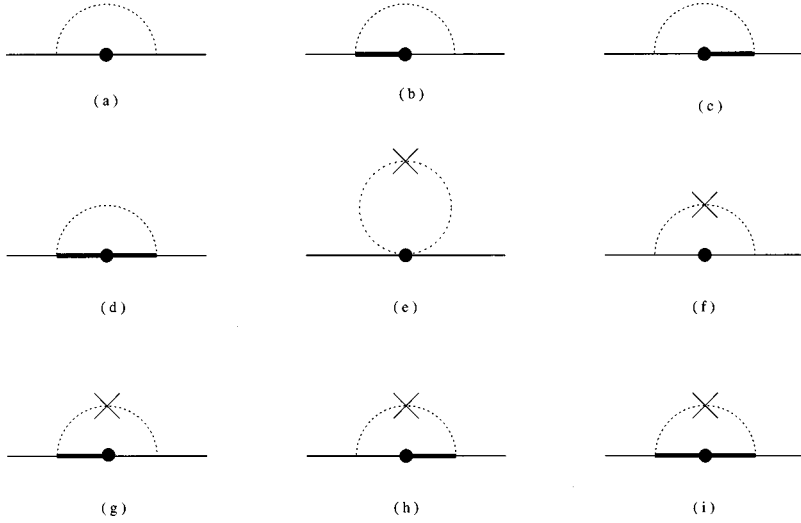
FIG. 3. Graphs contributing to the coefficients $\alpha^A_{ij,ab}$ and $\beta^A_{ij,ab}$. The solid dots represent the vertices stemming from the axial current. The cross represents the vertex $i(\alpha_\Phi p^2 - m_0^2)/3$.

cuplet states [16,17]. Since Jenkins and Manohar worked in the limit $m_u = m_d = 0$, we only need to consider additional contribution from nonzero $m_u(=m_d)$ for the comparison [14]. With this additional contribution, the full chiral perturbation theory result for g_A becomes

$$g_A = (D+F)\left[1 - \left\{1 + 2(D+F)^2\right.\right.$$

$$\left. + \frac{2C^2(9D+9F+25H)}{81(D+F)}\right\}\frac{M_\pi^2}{16\pi^2 f^2}\ln\frac{M_\pi^2}{\mu^2}$$

$$-\left\{\frac{1}{2} + \frac{15D^3 - D^2F + 3DF^2 + 33F^3}{6(D+F)}\right.$$

$$\left. + \frac{C^2(-27D+45F+20H)}{162(D+F)}\right\}\frac{M_K^2}{16\pi^2 f^2}\ln\frac{M_K^2}{\mu^2}$$

$$\left. - \frac{(-D+3F)^2}{3}\frac{M_\eta^2}{16\pi^2 f^2}\ln\frac{M_\eta^2}{\mu^2}\right]. \tag{3.10}$$

On the other hand, our result for the quenched g_A is

$$g_A^Q = (D+F)\left[1 + \left\{\frac{4(D-3F)(D^2+2DF+3D\gamma+3F\gamma)}{3(D+F)}\right.\right.$$

$$\left. + \frac{C^2(-15D+9F-10H)}{27(D+F)}\right\}\frac{M_\pi^2}{16\pi^2 f^2}\ln\frac{M_\pi^2}{\mu^2}$$

$$+ 2(-D+3F)^2\frac{1}{48\pi^2 f^2}\left\{(2\alpha_\Phi M_\pi^2 - m_0^2)\ln\frac{M_\pi^2}{\mu^2}\right.$$

$$\left.\left.\left. + (\alpha_\Phi M_\pi^2 - m_0^2)\right\}\right]\right], \tag{3.11}$$

which we can get easily from Eq. (3.4) using the fact that g_A is equal to the $\langle p|J^{1+i2}|n\rangle$ due to the isospin symmetry.

Note that in the quenched chiral calculations the meson loops with the s flavor do not contribute to this matrix element.

For a graphical comparison, we need to consider the values of various parameters in the above result. In full theory with octet states only, there are two free parameters D and F in Eq. (3.10). A χ^2 fit to the hyperon semileptonic decays gives $D \sim 0.56$ and $F \sim 0.33$. Additional contribution from the intermediate decuplet states introduces two additional parameters C^2 and H. Jenkins and Manohar determined the parameter C^2 by fitting the $\Delta \to N\pi$ decay rate $|C| \sim 1.6$. Three parameter fit yielded $D \sim 0.61$, $F \sim 0.40$, and $H \sim -1.9$. They used $\mu \sim 1$ GeV. The quenched chiral expressions for the axial currents given by Eq. (3.4) need seven parameters D, F, C^2, H, γ, α_Φ, and m_0. One way to determine the values of these parameters is to fit to the quenched lattice data for the axial currents obtained on the physical quark masses. However, since such simulation data is not yet available at present and we are only interested in the qualitative comparison between the full chiral and the quenched chiral behaviors of the physical quantities rather than actual values of the parameters, let us use the values for the parameters D, F, C^2, and H obtained by Jenkins and Manohar for the sake of comparison. Also, let us choose the physical η' mass for the value of the parameter m_0. We set the value of the parameter γ by the relation $\gamma = 2(D-F)$ and choose $\alpha_\Phi = 0$.

In Fig. 4, we show the full and the quenched chiral behaviors of the nucleon isovector axial charge with the octet states only and with both the octet and the decuplet states using the parameter values mentioned in the above (in the full chiral calculations, the K-π and the η-K mass differences are fixed at the physical values). The full χPT result with the octet states only gives noticeable pion mass dependence while the result with the octet and the decuplet states shows flatter behavior. On the other hand, both plots of the g_A^Q shows an almost flat behavior in the region $4m_\pi^{\text{physical}}$ and $6m_\pi^{\text{physical}}$. Interestingly, for the quenched case, the result with the octet states only is flatter. For the same values of the parameters, in Fig. 5 we compare the quenched theory result with the full theory result for degenerate quark mass case
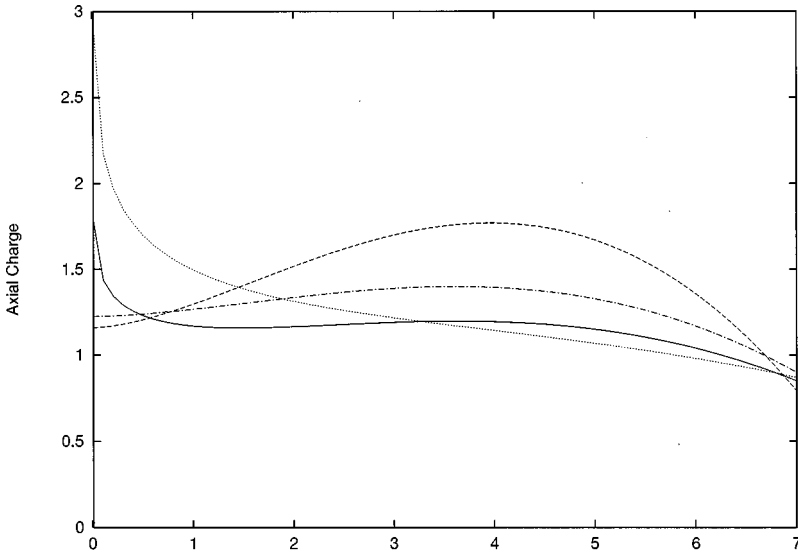
FIG. 4. Chiral behaviors of the nucleon isovector axial charge from QχPT and χPT with the intermediate states of the octet states and with the intermediate states of both the octet and the decuplet states. The solid, dotted, dashed, and dot-dashed lines show the chiral behaviors form QχPT with the octets, QχPT with the octets and the decuplets, χPT with the octets, and χPT with the octets and the decuplets, respectively. Here the horizontal axis represents $m_\pi/m_\pi^{\text{physical}}$ and ranges from 0.01 to 7.

$(m_\pi^2 = m_K^2 = m_\eta'^2)$, in order to see isolated effects from the quenched chiral singularity. There is not much difference between the full theory with nondegenerate quark masses (Fig. 4) and the full theory with degenerate quark masses (Fig. 5).

Although g_A^Q diverges as $m_\pi \to 0$ as expected, g_A^Q stays within $\sim 20\%$ of the experimental value for g_A around $m_\pi \sim m_\pi^{\text{physical}}$. This may be just due to a fortuitous choice of the parameters: our result varies less than 10% for the values $\gamma = 0 \sim 1$ and depends much more weakly on α_Φ (the variation is less than 3% for $\alpha_\Phi = -1 \sim +1$) and D (stable for $0.49 < D < 0.73$). On the other hand, the behavior of our result changes a lot as m_0^2 or F is changed (see Figs. 6 and 7) because the singular contribution is proportional to $(D - 3F)^2 m_0^2$.

Of course these results are reliable only for sufficiently small pion mass because the higher order corrections become important as the pion mass increases and the leading order result will be no longer valid. In the large m_π case, we should take our figures as suggestions for the possible m_π dependence. Quenched lattice simulation data of the axial charge exist [15] but the simulation was performed in the heavy pion mass region so we could not compare our one-loop result with the lattice data.

IV. DISCUSSIONS

To understand quenching effects on the axial charges of the octet baryons in QCD, we performed a one-loop correction to the axial charges using quenched chiral perturbation theory for baryons. In quenched QCD, the contribution from the disconnected quark diagrams vanishes and singlet meson η' remains light. This induces more singular chiral corrections $(m_0^2/48\pi^2 f^2)\ln(M_{aa'}^2/\mu^2)[\equiv \delta \ln(M_{aa'}^2/\mu^2)]$ to the matrix elements $\langle B_i | J^A | B_j \rangle$ than $(M^2/16\pi^2 f^2)\ln(M^2/\mu^2)$ ($M = m_\pi, m_K, m_\eta$) in full QCD. Therefore, similar to the observables considered by others, a quenching artifact to the axial charge also occurs as a leading singularity.

In particular, we compared QχPT result for g_A^Q with χPT result for g_A in detail. Beside the obvious fact that K and η loops do not contribute to the renormalization of g_A^Q in quenched theory (because they form disconnected quark dia-
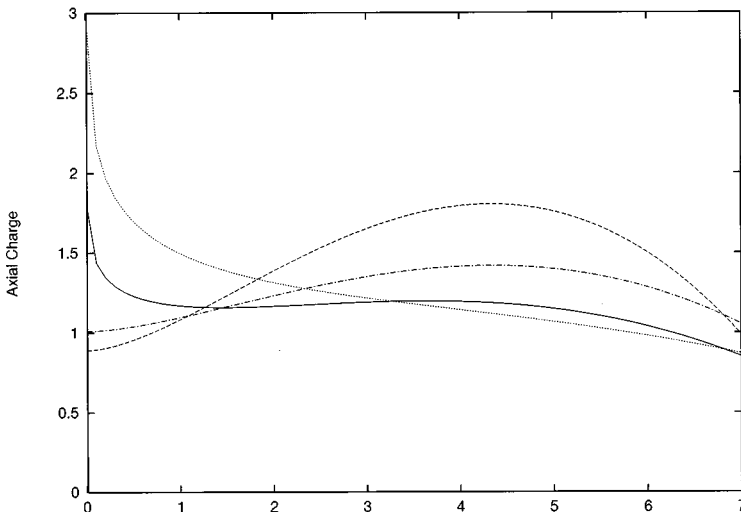
FIG. 5. Chiral behaviors of the nucleon isovector axial charge from QχPT and χPT for the degenerate quark masses $(m_\pi^2 = m_K^2 = m_\eta'^2)$. The meaning of the line types and the axes is the same as Fig. 4. The horizontal axis ranges from 0.01 to 7.
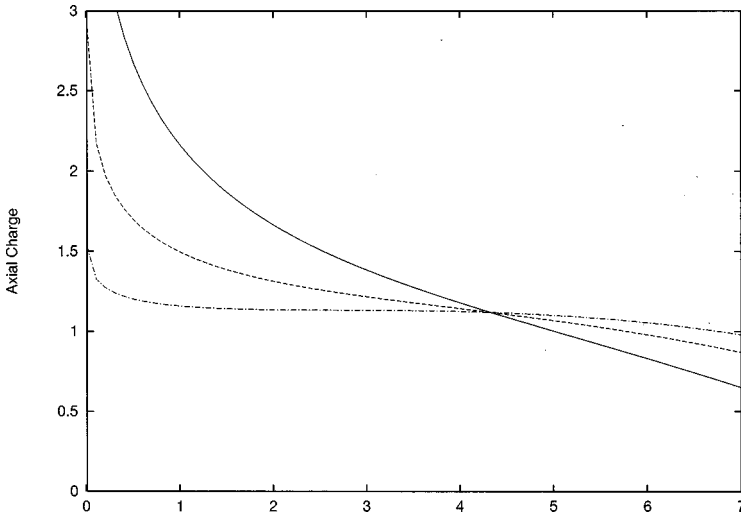
FIG. 6. Chiral behaviors of the nucleon isovector axial charge from QχPT with the octet and the decuplet states. The dot-dashed line is for $m_0 = 500$ MeV, the dotted line is for $m_0 = m'_\eta(960)$ MeV (the parameter chosen for Fig. 4), and the solid line is for $m_0 = 1500$ MeV. The horizontal axis ranges from 0.01 to 7.

grams), we found that in the limit $m_\pi \to 0$,

$$g_A^Q \to c^Q \ln m_\pi, \tag{4.1}$$

in contrast to full QCD chiral perturbation theory behavior,

$$g_A \to (D+F). \tag{4.2}$$

Since the chiral limit of the axial charges of the octet baryons g_A^Q in the quenched chiral perturbation theory is found to be singular, extrapolating the quenched lattice QCD calculation result of octet baryon axial charge to lighter quark mass would require careful consideration. Interestingly, our result does not depend on γ' even though there are two possible sources for the γ' dependence: one from the axial current [Eq. (3.1)] and the other from the Lagrangian [Eq. (2.17)]. This is because there is no γ' contribution from the axial current insertion because the γ' vertex in the current contains str (T^A) and vanishes. Thus, the tree level diagrams do not have γ' dependence. In one-loop level, wave function renormalization type Feynman diagrams [Figs. 2(b) and 2(d)] do not give the γ' dependence because only the interaction vertices involving the octet-meson decuplet (C)

can appear. Similarly, Figs. 3(b), 3(c), 3(g), and 3(h) do not depend on γ' because the interaction vertices in these diagrams do not have decuplet-meson-decuplet vertices. Figures 3(d) and 3(i) do not contribute to γ' dependence because the interaction vertices from the Lagrangian do not have decuplet-meson-decuplet vertices and the axial current insertion cannot have γ' dependence due to vanishing str (T^A).

In Sec. III, we calculated the chiral corrections to the axial charge assuming that the octet baryons and the decuplet baryons are degenerate ($\Delta M = 0$). In reality, this assumption does not hold and in the lattice QCD simulation the octet-decuplet mass splitting depends on the simulation parameters. Thus, we need to consider the $\Delta M \neq 0$ case. The effect of finite ΔM can be taken into consideration by modifying the decuplet baryon propagator from $iP_{\mu\nu}/v \cdot k$ to $iP_{\mu\nu}/(v \cdot k \pm \Delta M)$ (where $P_{\mu\nu}$ is the projection operator for the spin-3/2 field $v_\mu v_\nu - g_{\mu\nu} - 4/3S_\mu S_\nu$) for those Feynman diagrams which involve decuplet baryon propagators. For these Feynman diagrams, flavor factors and vertices stay the same as in the $\Delta M = 0$ case. We can expand this modified decuplet baryon propagator for small ΔM. Then, up to $\mathcal{O}(\Delta M)$, X_{ab}, Y_{ab}, Y_{aa} for those terms which involve C^2 in Eq. (3.4) are replaced by
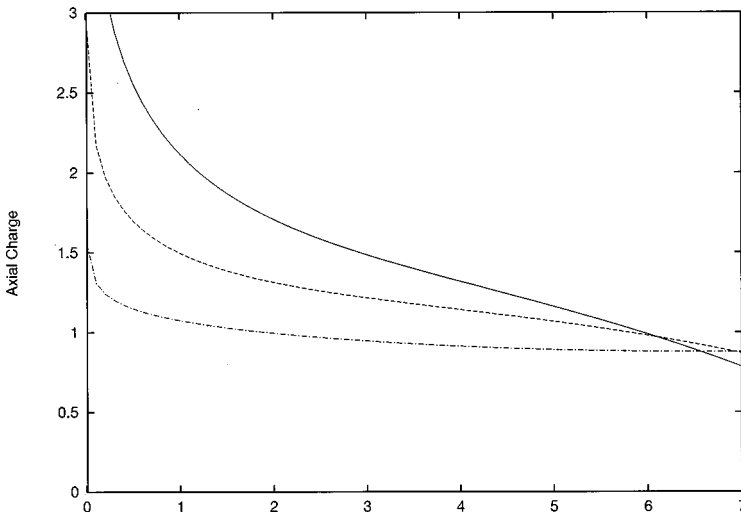
FIG. 7. Chiral behaviors of the nucleon isovector axial charge from QχPT with the octet and the decuplet states. The dot-dashed line is for $F = 0.32$, and the dotted line is for $F = 0.40$ (the parameter chosen for Fig. 4), and the solid line is for $F = 0.48$. The horizontal axis ranges from 0.01 to 7.

$$X'_{ab} = X_{ab} \pm n \frac{M_{ab} \Delta M}{16\pi f^2}, \tag{4.3}$$

$$Y'_{ab} = Y_{ab} \pm n \alpha_\Phi \frac{(M_a + M_b) \Delta M}{48\pi f^2}, \tag{4.4}$$

$$Y'_{aa} = Y_{aa} \pm 2n \alpha_\Phi \frac{M_{aa} \Delta M}{48\pi f^2}, \tag{4.5}$$

where n is equal to 1 for the contributions from Figs. 3(b), 3(c), 3(g), and 3(h) or 2 for those from Figs. 2(b), 2(d), 3(d), and 3(i). This correction is small in present lattice QCD simulations.

ACKNOWLEDGMENTS

APPENDIX A: EXPRESSIONS FOR THE AXIAL CURRENT RENORMALIZATIONS

Here we give the expressions for the coefficients appearing in Eq. (3.4). The expressions for t_{ij}^A are

$$t_{pp}^8 = \frac{-D + 3F}{2\sqrt{3}}, \quad t_{pn}^{1+i2} = D + F, t_{\Lambda\Sigma^-}^{1+i2} = \sqrt{\frac{2}{3}} D,$$

$$t_{\Xi^0\Xi^-}^{1+i2} = D - F, \quad t_{p\Lambda}^{4+i5} = -\frac{D + 3F}{\sqrt{6}},$$

$$t_{\Lambda\Xi^-}^{4+i5} = \frac{-D + 3F}{\sqrt{6}}, \quad t_{n\Sigma^-}^{4+i5} = D - F,$$

$$t_{\Sigma^0\Xi^-}^{4+i5} = \frac{D + F}{\sqrt{2}} = \frac{1}{\sqrt{2}} t_{\Sigma^+\Xi^0}^{4+i5}. \tag{A1}$$

The coefficients $\lambda_{ij,ab}$ and $\rho_{ij,ab}$ are defined by

$$\lambda_{ij,ab} = (\lambda_{i,ab} + \lambda_{j,ab})/2,$$

$$\rho_{ij,ab} = (\rho_{i,ab} + \rho_{j,ab})/2. \tag{A2}$$

The diagrams (a) and (b) in Fig. 2 yield

$$\lambda_{\Lambda,uu} = -\frac{1}{3} D^2 + 4DF - 3F^2 - (4D - 6F)\gamma + \frac{1}{2} C^2,$$

$$\lambda_{\Lambda,us} = -5D^2 + 2DF + 3F^2 + \frac{1}{2} C^2,$$

$$\lambda_{\Lambda,ss} = (D + 3F)\gamma, \tag{A3}$$

$$\lambda_{\Sigma,uu} = -D^2 + 3F^2 + 6F\gamma + \frac{1}{6} C^2,$$

$$\lambda_{\Sigma,us} = -D^2 + 6DF - 3F^2 + \frac{5}{6} C^2,$$

$$\lambda_{\Sigma,ss} = 3(-D + F)\gamma, \tag{A4}$$

$$\lambda_{N,uu} = \lambda_{\Sigma,uu} + \lambda_{\Sigma,us} + \lambda_{\Sigma,ss}, \quad \lambda_{N,us} = \lambda_{N,ss} = 0, \tag{A5}$$

$$\lambda_{\Xi,uu} = \lambda_{\Sigma,ss}, \quad \lambda_{\Xi,us} = \lambda_{\Sigma,us}, \quad \lambda_{\Xi,ss} = \lambda_{\Sigma,uu}. \tag{A6}$$

The diagrams (c) and (d) in Fig. 2 yield

$$\rho_{\Lambda,uu} = -\frac{3}{2} \left(\frac{4}{3} D - 2F \right)^2,$$

$$\rho_{\Lambda,us} = 3 \left(\frac{4}{3} D - 2F \right) \left(\frac{1}{3} D + F \right), \quad \rho_{\Lambda,ss} = -\frac{3}{2} \left(\frac{1}{3} D + F \right)^2 \gamma, \tag{A7}$$

$$\rho_{\Sigma,uu} = -6F^2 - \frac{1}{3} C^2,$$

$$\rho_{\Sigma,us} = 6F(D - F) + \frac{2}{3} C^2,$$

$$\rho_{\Sigma,ss} = -\frac{3}{2} (D - F)^2 - \frac{1}{3} C^2, \tag{A8}$$

$$\rho_{N,uu} = \rho_{\Sigma,uu} + \rho_{\Sigma,us} + \rho_{\Sigma,ss}, \quad \rho_{N,us} = \rho_{N,ss} = 0, \tag{A9}$$

$$\rho_{\Xi,uu} = \rho_{\Sigma,ss}, \quad \rho_{\Xi,us} = \rho_{\Sigma,us}, \quad \rho_{\Xi,ss} = \rho_{\Sigma,uu}. \tag{A10}$$

The $\alpha_{ij,ab}^A$ corresponds to the diagrams without the hairpin in Fig. 3. Our result for $\alpha_{ij,ab}^A$ is

$$\alpha_{pn,uu}^{1+i2} = \frac{2D(D - 3F)(-D + F)}{3(D + F)} + (D - 3F)\gamma + \frac{2C^2(6D + 18F - 5H)}{27(D + F)},$$

$$\alpha_{pn,us}^{1+i2} = \alpha_{pn,ss}^{1+i2} = 0, \tag{A11}$$

$$\alpha_{\Lambda\Sigma^-,uu}^{1+i2} = \frac{4D(-D + 3F)}{9} + \frac{2(D - 3F)\gamma}{3} + \frac{C^2(-6D + 18F - 18\gamma - 5H)}{54D},$$

$$\alpha_{\Lambda\Sigma^-,us}^{1+i2}=\frac{D(D-3F)}{9}+\frac{C^2(48D+72F-5H)}{108D},$$

$$\alpha_{\Lambda\Sigma^-,ss}^{1+i2}=\frac{(D-3F)\gamma}{3}+\frac{C^2\gamma}{3D}, \tag{A12}$$

$$\alpha_{\Xi^0\Xi^-,uu}^{1+i2}=(D-F)\gamma+\frac{-4C^2\gamma}{9(D-F)},$$

$$\alpha_{\Xi^0\Xi^-,us}^{1+i2}=\frac{-D^3+3D^2F-27DF^2+9F^3}{9(-D+F)}+\frac{C^2(18D+18F+5H)}{81(D-F)},$$

$$\alpha_{\Xi^0\Xi^-,ss}^{1+i2}=\frac{D^3+3D^2F+9DF^2-9F^3}{9(-D+F)}-2F\gamma+\frac{C^2(72F+72\gamma+5H)}{162(D-F)}, \tag{A13}$$

$$\alpha_{p\Lambda,uu}^{4+i5}=\frac{D^3+45D^2F-81DF^2+27F^3}{18(D+3F)}+\frac{(7D-15F)\gamma}{6}+\frac{C^2(9D+9F-5H)}{9(D+3F)},$$

$$\alpha_{p\Lambda,us}^{4+i5}=\frac{-25D^3+63D^2F-27DF^2-27F^3}{18(D+3F)}+\frac{-[C^2(6D-18F+5H)]}{18(D+3F)},$$

$$\alpha_{p\Lambda,ss}^{4+i5}=\frac{-[(D+3F)\gamma]}{6}, \tag{A14}$$

$$\alpha_{\Lambda\Xi^-,uu}^{4+i5}=\frac{(-D+F)(5D^2-6DF+9F^2)}{6(-D+3F)}+\frac{(7D-9F)\gamma}{6}+\frac{C^2(-9D+9F-18\gamma-5H)}{27(-D+3F)},$$

$$\alpha_{\Lambda\Xi^-,us}^{4+i5}=\frac{4D(D^2+6DF-9F^2)}{9(-D+3F)}+\frac{2C^2(3D-9F-5H)}{27(-D+3F)},$$

$$\alpha_{\Lambda\Xi^-,ss}^{4+i5}=\frac{(D+3F)(-5D^2+6DF-9F^2)}{18(-D+3F)}-\frac{(D+9F)\gamma}{6}+\frac{C^2(D+3F+6\gamma)}{9(-D+3F)}, \tag{A15}$$

$$\alpha_{n\Sigma^-,uu}^{4+i5}=\frac{D^3+9D^2F-9DF^2-9F^3}{18(-D+F)}+\frac{(D-5F)\gamma}{2}+\frac{C^2(9D+45F+18\gamma+5H)}{81(D-F)},$$

$$\alpha_{n\Sigma^-,us}^{4+i5}=\frac{-D^3+3D^2F-27DF^2+9F^3}{18(-D+F)}+\frac{C^2(18D+18F+5H)}{162(D-F)},$$

$$\alpha_{n\Sigma^-,ss}^{4+i5}=\frac{(D-F)\gamma}{2}+-2\frac{C^2\gamma}{9(D-F)}, \tag{A16}$$

$$\alpha_{\Sigma^0\Xi^-,uu}^{4+i5}=\frac{(D-F)(-D^2+6DF+3F^2)}{6(D+F)}+\frac{(D-3F)\gamma}{2}+\frac{C^2(-9D+9F-5H)}{81(D+F)},$$

$$\alpha_{\Sigma^0\Xi^-,us}^{4+i5}=\frac{(-D+F)(D^2+3F^2)}{3(D+F)}+\frac{2C^2(27D+45F-10H)}{81(D+F)},$$

$$\alpha_{\Sigma^0\Xi^-,ss}^{4+i5}=\alpha_{\Sigma^0\Xi^-,uu}^{4+i5}, \tag{A17}$$

$$\alpha_{\Sigma^+\Xi^0,ab}^{4+i5}=\alpha_{\Sigma^0\Xi^-,ab}^{4+i5}, \tag{A18}$$

$$\alpha_{pp,uu}^{8}=\frac{2D(D-3F)}{3}+(D-3F)\gamma+5\frac{C^2H}{9(D-3F)},\quad \alpha_{pp,us}^{8}=\alpha_{pp,ss}^{8}=0. \tag{A19}$$

The diagrams with the hairpin in Fig. 3 yield the following results for $\beta_{ij,ab}^A$:

$$\beta_{pn,uu}^{1+i2}=\frac{(-D+3F)^2}{2}, \quad \beta_{pn,us}^{1+i2}=\beta_{pn,ss}^{1+i2}=0, \tag{A20}$$

$$\beta_{\Lambda\Sigma^-,uu}^{1+i2}=\frac{2F(-2D+3F)}{3}+2\frac{C^2(-2D+3F)}{9D},$$

$$\beta_{\Lambda\Sigma^-,us}^{1+i2}=\frac{2(D^2-2DF+3F^2)}{3}+\frac{C^2(5D-3F)}{9D},$$

$$\beta_{\Lambda\Sigma^-,ss}^{1+i2}=\frac{-D^2}{6}-\frac{DF}{3}+\frac{F^2}{2}+\frac{-[C^2(D+3F)]}{9D}, \tag{A21}$$

$$\beta_{\Xi^0\Xi^-,uu}^{1+i2}=\frac{(D-F)^2}{2}+\frac{C^2(-36D+36F-5H)}{81(D-F)},$$

$$\beta_{\Xi^0\Xi^-,us}^{1+i2}=-2(D-F)F+\frac{2C^2(18D+18F+5H)}{81(D-F)},$$

$$\beta_{\Xi^0\Xi^-,ss}^{1+i2}=2F^2+\frac{-[C^2(72F+5H)]}{81(D-F)}, \tag{A22}$$

$$\beta_{p\Lambda,uu}^{4+i5}=\frac{1}{4}+\frac{2D^2}{3}-3DF+3F^2,$$

$$\beta_{p\Lambda,us}^{4+i5}=-\frac{1}{2}+\frac{-D^2}{6}+\frac{3F^2}{2},$$

$$\beta_{p\Lambda,ss}^{4+i5}=\frac{1}{4}, \tag{A23}$$

$$\beta_{\Lambda\Xi^-,uu}^{4+i5}=\frac{1}{4}+\frac{2D^2-5DF+3F^2}{3}+\frac{4C^2(-2D+3F)}{9(-D+3F)},$$

$$\beta_{\Lambda\Xi^-,us}^{4+i5}=-\frac{1}{2}+\frac{-D^2-10DF+15F^2}{6}+\frac{2C^2(5D-3F)}{9(-D+3F)},$$

$$\beta_{\Lambda\Xi^-,ss}^{4+i5}=\frac{1}{4}+\frac{F(D+3F)}{3}+\frac{2C^2(D+3F)}{9(D-3F)}, \tag{A24}$$

$$\beta_{n\Sigma^-,uu}^{4+i5}=\frac{1}{4}+F(-D+3F)+\frac{2C^2(D-3F)}{9(D-F)},$$

$$\beta_{n\Sigma^-,us}^{4+i5}=-\frac{1}{2}+\frac{D^2-4DF+3F^2}{2}+\frac{2C^2(D-3F)}{9(-D+F)},$$

$$\beta_{n\Sigma^-,ss}^{4+i5}=\frac{1}{4}, \tag{A25}$$

$$\beta_{\Sigma^0\Xi^-,uu}^{4+i5}=\frac{1}{4}+F(-D+F)+\frac{2C^2(-9D-9F+5H)}{81(D+F)},$$

$$\beta^{4+i5}_{\Sigma^0\Xi^-,us} = -\frac{1}{2} + \frac{D^2-2D+5F^2}{2} + \frac{4C^2(9D+9F-5H)}{81(D+F)},$$

$$\beta^{4+i5}_{\Sigma^0\Xi^-,ss} = \frac{1}{4} + F(-D+F) + \frac{2C^2(-9D-9F+5H)}{81(D+F)}, \tag{A26}$$

$$\beta^{4+i5}_{\Sigma^+\Xi^0,ab} = \beta^{4+i5}_{\Sigma^0\Xi^-,ab}, \tag{A27}$$

$$\beta^8_{pp,uu} = \frac{(-D+3F)^2}{2}, \quad \beta^8_{pp,us} = \beta^8_{pp,ss} = 0. \tag{A28}$$

[1] See for example, Nucl. Phys. B (Proc. Suppl.) **47**, (1996); **53** (1997).

[2] S. Sharpe, Phys. Rev. D **41**, 3233 (1990); **46**, 3146 (1992).

[3] C. Bernard and M.F.L. Golterman, Phys. Rev. D **46**, 853 (1992); **49**, 486 (1994).

[4] A. Morel, J. Phys. (Paris) **48**, 1111 (1987).

[5] J.N. Labrenz and S. Sharpe, Phys. Rev. D **54**, 4595 (1996).

[6] S. Kim and D. K. Sinclair, Phys. Rev. D **52**, R2614 (1995).

[7] R. Gupta, Nucl. Phys. B (Proc. Suppl.) **42**, 85 (1995).

[8] R. Mawhinney, Nucl. Phys. B (Proc. Suppl.) **47**, 557 (1996).

[9] S. Sharpe, Nucl. Phys. B (Proc. Suppl.) **53**, 181 (1997).

[10] M. J. Booth, Phys. Rev. D **51**, 2338 (1995).

[11] S. R. Sharpe and Y. Zhang, Phys. Rev. D **53**, 5125 (1996).

[12] C. Bernard and M.F.L. Golterman, Phys. Rev. D **53**, 476 (1996).

[13] H. Georgi, Phys. Lett. B **240**, 447 (1990).

[14] M.A. Luty and M. White, Phys. Lett. B **319**, 261 (1993).

[15] K.F. Liu, S.J. Dong, T. Draper, and J.M. Wu, Phys. Rev. D **49**, 4755 (1994).

[16] E. Jenkins and A.V. Manohar, Phys. Lett. B **255**, 558 (1991).

[17] E. Jenkins and A.V. Manohar, Phys. Lett. B **259**, 353 (1991).